PHOTOCATALYTIC REMOVAL OF METHYLENE BLUE FROM AQUEOUS SOLUTION BY Ag AND La DOPED TiO₂ AND ZEOLITE SUPPORTED TiO₂ UNDER VISIBLE LIGHT

by

NAJM US SAQIB

Thesis submitted in fulfilment of the requirements

for the degree of

Doctor of Philosophy

August 2017

ACKNOWLEDGEMENT

I would like to express my sincere gratitude to my supervisor; Prof. Dr. Rohana Adnan for her guidance, insightful comments, encouragement, consistent and endless support throughout my research work. I have been extremely lucky to have a supervisor who cared so much about my work, and who responded to my questions and queries so promptly. It was a real privilege and an honour for me to share her exceptional scientific knowledge but also of her extraordinary human qualities.

I must express my gratitude to my parents, family members and relatives who experienced all of the ups and downs of my life. An especially warm and sincere thank you goes to my mother and family for their constant encouragement, love and prayers, as well as moral and spiritual support.

I would like to thank my lab-fellows; Irfan, Jaga, Fitra and Farah, for their support and helps. I would also like to thank all the members of staff at Universiti Sains Malaysia.

Last but not least, I would like to thank the The World Academy of Sciences (TWAS) and Universiti Sains Malaysia (USM) for the award of 2012-TWAS-USM-Postgraduate-Fellowship (FR number: 3240268486) which allowed me to undertake this research.

TABLE OF CONTENTS

AC	KNOWL	.EDGE1	MENT	ii
TAì	BLE OF	CONTE	ENTS	iii
LIS	T OF TA	BLES.		vi
LIS	T OF FIG	GURES		ix
LIS	T OF AE	BERE	VIATIONS	xiv
AB	STRAK.			xv
ABS	STRACT	`		xvii
CH	APTER	1 - INT	RODUCTION	1
1.1	Backgro	und	•••••••••••••••••••••••••••••••••••••••	1
			ents	
1.3	Objectiv	es of th	e Proposed Work	5
CH	APTER	2 - LIT	ERATURE REVIEW	7
		-		
2.2	Titaniun	n Dioxi	de	10
2.3	Modific	ations o	f TiO ₂	12
	2.3.1	Doping	3	12
		2.3.1(a)Anionic (Non-metals) Doping	14
		2.3.1(b)Cationic (Metals) Doping	15
		2.3.1(c	Co-doping	18
	2.3.2	Modifi	cations with Dye Sensitization and Coupling	20
	2.3.3	Modifi	cations via Calcination Temperature	21
2.4	Immobi	lization	of TiO ₂ onto Solid Support	23
	2.4.1	Immol	oilization of TiO ₂ onto Zeolite Solid Support	25
2.5	Photoca	talytic 1	Applications of TiO ₂	27
		2.5.1	Identification of the Primary Oxidant in TiO2 Photocatalys	sis 29
			2.5.1(a)Photocatalytic Degradation of Methylene Blue by	TiO2
				32
	2.5.2	Photo	catalytic Reduction/Adsorption of Metal Ions by TiO2	34
CH	APTER	3 - MA	TERIALS AND METHODS	36

3.1	Chemica	al Reagents	36
3.2	Preparat	ion of TiO ₂ NPs	36
	3.2.1	Preparation of Metals Doped TiO ₂ NPs	37
	3.2.2	Preparation of Zeolite Supported Pure and Metal doped TiO ₂ NPs	37
3.3	Characte	erizations	38
	3.3.1	X-ray Diffraction Analysis	38
	3.3.2	Scanning Electron Microscopy (SEM) Analysis	38
	3.3.3	Energy Dispersive X-ray (EDX) and X-ray Fluorescence Spectrometer	er
		Analyses	. 39
	3.3.4	Transmission Electron Microscopy (TEM) Analysis	40
	3.3.5	UV-Vis Diffused Reflectance Spectroscopy (DRS) Analysis	. 40
	3.3.6	Fourier Transform Infrared Spectroscopy	. 40
	3.3.7	UV-Visible Spectroscopy	. 41
	3.3.8	Atomic Absorption Spectroscopy	. 41
	3.3.9	Determination of the pH of Point of Zero Charge (pH _{PZC})	. 41
3.4	Evaluati	on of Photocatalytic Efficiency	. 42
	3.4.1	Evaluation of the Effect of Photocatalysts Dosage	. 43
	3.4.2	Evaluation of the Effect of Initial Concentrations of MB	. 43
	3.4.3	Evaluation of the Effect of pH	. 43
	3.4.4	Evaluation of the Effect of Competitive Ions Addition Cd ²⁺ , on the	
		Removal of MB	. 44
	3.4.5	Batch Kinetic Study	. 44
	3.4.6	Batch Adsorption Isotherm Studies	. 46
3.5	Regener	ration of Spent Photocatalysts	. 48
СН	APTER	4 - CHARACTERIZATIONS OF DOPED AND UNDOPED TIO	2
		AND ZEOLITE SUPPORTED TiO2 NPs	50
		ction	
4.2	Charact	erizations	
	4.2.1	X-ray Diffraction Analysis	51

	4.2.2	Electron Microscopic Analyses 59			
	4.2.3	Chemical State and Elemental Composition Analyses			
	4.2.4	UV-Vis Diffused Reflectance Spectroscopy (DRS) Analysis			
	4.2.5	Fourier Transform Infrared Spectroscopy (FTIR) Analysis			
	4.2.6	Determination of pH of Point of Zero Charge (pH _{PZC}) 82			
СН	APTER	5 - PHOTO-DEGRADATION OF METHYLENE BLUE BY			
		DOPED AND UNDOPED TiO2 AND ZEOLITE SUPPORTED			
		TiO ₂			
5.2	Photoca	talysts Dosage Optimization			
5.3	Evaluati	on of the Effects of MB Initial Concentrations			
5.4	Evaluati	on of the Effect of pH on the Photo-Degradation of MB94			
5.5	5.5 Effect of Competitive Ion (Cd ²⁺) on the Photo-Degradation of MB				
5.6	Equilibr	ium Study of MB Photo-Degradation			
5.7	Batch K	inetic Study			
5.8	Batch A	dsorption Isotherm Study			
5.9	9 Verification of the Mechanism of MB Photo-Degradation				
	5.9.1	FT-IR Analysis of Spent Photocatalysts			
	5.9.2	EDX and XRF Analyses of Spent Photocatalysts			
5.10) Regene	ration Study of Used Photocatalyst137			
СН	APTER	6 - CONCLUSIONS AND RECOMENDATIONS 142			
6.1	Conclus	tions Derived from the Current Work			
6.2	Future F	Recommendations for the Extension of Present Work			
RE	FEREN	CES145			
AP.	APPENDICES				
LIS	T OF P	UBLICATIONS AND CONFERENCE PRESENTATION			

LIST OF TABLES

	1	Page
Table 2.1	Comparative MB removal efficiencies of various modified TiO ₂	33
	photocatalysts	
Table 4.1	Particle size and phase composition of doped and undoped TiO2	54
	and zeolite supported TiO2 NPs calcined at different temperatures	
Table 4.3	Elemental composition of unsupported doped and undoped TiO2	70
	NPs	
Table 4.4	Elemental composition zeolite supported doped and undoped	71
	zeolite supported TiO ₂ NPs	
Table 4.5	Calculated direct and indirect band gap energy values of doped	77
	and undoped TiO2 and zeolite supported TiO2 NPs	
Table 4.6	pH of point of zero charge (pH _{PZC}) of doped and undoped TiO ₂	83
	and zeolite supported TiO ₂ NPs	
Table 5.1	The photo-degradation efficiency of MB ($[MB]_o = 30 \text{ mg/L}$) at	88
	various dosage of doped and undoped TiO2 NPs at pH 6.8±0.1,	
	and at different pH by using prepared at different calcination	
	temperatures	
Table 5.2	The photo-degradation efficiency of MB ([MB] $_{o}$ = 150 mg/L) at	89
	various dosage of doped and undoped zeolite supported TiO2 NPs	
	at pH 6.8±0.1, and at different pH by using prepared at different	
	calcination temperatures	
Table 5.3	The comparison on the effect of MB intial concentrations on the	91
	removal efficiency of doped and undoped TiO2 NPs prepared at	
	different calcination temperatures, exposed to compact fluorescent	
	light for 3 h	
Table 5.4	The comparison on the effect of MB intial concentrations on the	91
	removal efficiency of doped and undoped zeolite supported TiO2	
	NPs prepared at different calcination temperatures, exposed to	
	compact fluorescent light for 3 h	
Table 5.5	The comparison of the effect of pH on the removal efficiency of	97
	MB onto doped and undoped TiO2 NPs prepared at different	

	calcination temperatures, exposed to compact fluorescent light for	
	3 h	
Table 5.6	The comparison of the effect pH on the removal efficiency of MB	97
	onto doped and undoped zeolite supported TiO2 NPs prepared at	
	different calcination temperatures, exposed to compact fluorescent	
	light for 3 h	
Table 5.7	Removal efficiency (%) of MB using doped and undoped TiO2, at	100
	various initial concentrations of Cd2+ ions, using 0.2 g of	
	photocatalysts, conducted at pH 6.8±0.1 and exposed under	
	compact fluorescent light for 3 h	
Table 5.8	Removal efficiency (%) of MB using doped and undoped zeolite	100
	supported TiO ₂ , at various initial concentration of Cd ²⁺ ions, using	
	0.2 g of photocatalysts, conducted at pH 6.8±0.1 and exposed	
	under compact fluorescent light for 3 h	
Table 5.9	Comparison of MB maximum adsorption and removal capacity	111
	onto different modified TiO ₂ adsorbents and that of unsupported	
	and supported TiO ₂ NPs	
Table 5.10	Comparison of physico-chemical properties of TiO ₂ prepared by	114
	LI, sol-gel and pre-sulphated methods	
Table 5.11	Kinetic parameters of the photocatalytic adsorption of MB ([MB] _o	120
	= 30 mg/L) using 0.2 g doped and undoped TiO ₂ NPs at 25±2 °C,	
	conducted at pH 6.8±0.1 and exposed under compact fluorescent	
	light for 3 h	
Table 5.12	Kinetic parameters for the adsorption of MB ($[MB]_o = 150 \text{ mg/L}$)	121
	using 0.2 g doped and undoped zeolite supported TiO2 NPs at	
	25±2 °C, conducted at pH 6.8±0.1 and exposed under compact	
	fluorescent light for 3 h	
Table 5.13	Intraparticle diffusion model parameters for the adsorption of MB	122
	$([MB]_o = 30 \text{ mg/L}) \text{ onto TiO}_2 \text{ and doped TiO}_2 \text{ NPs}$	
Table 5.14	Intraparticle diffusion model parameters for the adsorption of MB	122
	([MB] = 150 mg/L) onto zeolite supported TiO ₂ NPs	

Table 5.15	Langmuir and Freundlich adsorption isotherm parameters of MB	128
	adsorption by 0.2 g of doped and undoped TiO2 NPs, conducted at	
	pH 6.8±0.1 and exposed under compact fluorescent light for 3 h	
Table 5.16	Langmuir and Freundlich adsorption isotherm parameters of MB	129
	adsorption by 0.2 g of doped and undoped zeolite supported ${\rm TiO_2}$	
	NPs, conducted at pH 6.8±0.1 and exposed under compact	
	fluorescent light for 3 h	
Table 5.17	Comparison of the elemental composition of fresh and used doped	135
	and undoped TiO ₂ NPs calcined at 500 °C by using EDX and XRF	
	analyses	
Table 5.18	Comparison of the elemental composition of fresh and used doped	136
	and undoped zeolite supported TiO2 NPs calcined at 500 °C by	
	using EDX and XRF analyses	

LIST OF FIGURES

		Page
Figure 2.1	Schematic band structure of crystalline TiO2 for direct and	9
	indirect electronic transitions	
Figure 2.2	Bulk structures of rutile and anatase TiO ₂ (Diebold, 2003)	11
Figure 2.3	Schematic representation of mid band gap energy state and	14
	Fermi level (EF) (Ruzicka, 2013)	
Figure 2.4	Schematic representation of Bickley's (Bickley et al., 1991),	23
	and Hurum's theories (Hurum et al., 2003)	
Figure 2.5	Photo-induced excitation and de-excitation mechanism of	30
	semiconductor photocatalyst (TiO ₂) (Diesen, 2013)	
Figure 2.6	Chemical structure of Methylene Blue (MB) dye	33
Figure 4.1	Photo-excitations of TiO ₂ NPs in presence of doped metal ion	51
Figure 4.2	XRD patterns of doped and Ag doped TiO2 and zeolite	56
	supported TiO ₂ NPs at different calcination temperatures	
Figure 4.3	XRD patterns of Ag-La doped and La doped TiO2 and zeolite	57
	supported TiO ₂ NPs at different calcination temperatures	
Figure 4.4	Percent (wt %) rutile and brookite phases with respect to	59
	particle sizes of doped and undoped (a) TiO2, and (b) zeolite	
	supported TiO ₂ NPs prepared at different calcination	
	temperatures	
Figure 4.5	SEM images of (a) TiO ₂ , (b) Ag/TiO ₂ , (c) Ag-La/TiO ₂ , (d)	61
	La/TiO_2 , (e) $Z@TiO_2$, (f) $Z@Ag/TiO_2$, (g) $Z@Ag-La/TiO_2$, (h)	
	Z@La/TiO ₂ calcined at 500 °C, respectively	
Figure 4.6	SEM images of (a) TiO ₂ , (b) Ag/TiO ₂ , (c) Ag-La/TiO ₂ , (d)	62
	La/TiO_2 , (e) $Z@TiO_2$, (f) $Z@Ag/TiO_2$, (g) $Z@Ag-La/TiO_2$, (h)	
	Z@La/TiO ₂ calcined at 700 °C, respectively	
Figure 4.7	SEM and TEM images of zeolite supported TiO ₂ calcined at	64
	900 °C, (a) SEM, Z@Ag/TiO ₂ , (b) SEM, Z@TiO ₂ , (c) TEM,	
	$Z@Ag/TiO_2$, and (d) $Z@TiO_2$	

Figure 4.8	TEM images of (a) TiO ₂ , (b) Ag/TiO ₂ , (c) Ag-La/TiO ₂ , (d)	65
	La/TiO_2 , (e) $Z@TiO_2$, (f) $Z@Ag/TiO_2$, (g) $Z@Ag-La/TiO_2$, (h)	
	Z@La/TiO ₂ calcined at 500 °C, respectively	
Figure 4.9	TEM images of (a) TiO ₂ , (b) Ag/TiO ₂ , (c) Ag-La/TiO ₂ , (d)	66
	La/TiO_2 , (e) $Z@TiO_2$, (f) $Z@Ag/TiO_2$, (g) $Z@Ag-La/TiO_2$,	
	and (h) Z@La/TiO2 calcined at 700 °C, respectively	
Figure 4.10	XPS spectra of the major peaks for (a) Ag 3d, (b) O 1s, and (c)	68
	Ti 2p, respectively	
Figure 4.11	EDX spectra of (a) TiO ₂ , (b) Z@TiO ₂ , (c) Ag/TiO ₂ , (d)	72
	$Z@Ag/TiO_2$, (e) $Ag-La/TiO_2$, (f) $Z@Ag-La/TiO_2$, (g) La/TiO_2 ,	
	(h) Z@La/TiO ₂ calcined at 500 °C, respectively	
Figure 4.12	DRS (UV-Vis) spectra of doped and undoped (a) TiO2, and (b)	75
	zeolite supported TiO2 NPs calcined at different temperatures	
Figure 4.13	DR UV-Vis spectra for direct electronic transition (a) and (c)	78
	and indirect transition of (b) and (d) unsupported TiO2 and	
	Ag/TiO ₂ , respectively	
Figure 4.14	DR UV-Vis spectra for direct electronic transition (a) and (c)	78
	and indirect transition of (b) and (d) for Z@TiO2 and	
	Z@Ag/TiO2, respectively	
Figure 4.15	DR UV-Vis spectra for direct electronic transition (a) and (c)	79
	and indirect transition of (b) and (d) for Ag-La/TiO2 and	
	La/TiO ₂ , respectively	
Figure 4.16	DR UV-Vis spectra for direct electronic transition (a) and (c),	79
	and indirect transition of (b) and (d) for Z@Ag-La/TiO2 and	
	Z@La/TiO ₂ , respectively	
Figure 4.17	FT-IR spectra of doped and undoped (a) TiO ₂ and (b) zeolite	81
	supported TiO ₂ NPs	
Figure 4.18	pH of point of zero charge (pH _{PZC}) of doped and undoped (a)	84
	TiO ₂ and (b) zeolite supported TiO ₂ NPs	
Figure 5.1	Dose optimization of doped and undoped (a) TiO_2 ([MB] _o = 30	86
	mg/L), (b) zeolite supported TiO_2 NPs ([MB] _o = 150 mg/L),	
	respectively	

Figure 5.2	Effect of MB initial concentrations on photocatalytic	92
	degradation of doped and undoped (a) TiO2, and (b) zeolite	
	supported TiO2 NPs, at dosage 0.2 g, pH 6.8±0.1 and under	
	compact fluorescent light for 3 h	
Figure 5.3	Comparison of MB degradation by doped and undoped (a)	101
	TiO ₂ , and (b) zeolite supported TiO ₂ NPs, using 0.2 g of	
	photocatalysts, conducted at pH 6.8±0.1, exposed under	
	compact fluorescent light for 3 h, and with (1:1 ratio) and	
	without competitive Cd2+ ions	
Figure 5.4	Removal efficiency (%) of (a) Ag/TiO ₂ , and (b) Ag-La/TiO ₂	103
	NPs towards different concentrations of Cd2+ and MB, using	
	0.2 g of photocatalysts, conducted at pH 6.8±0.2 and exposed	
	under compact fluorescent light for 3 h	
Figure 5.5	Removal efficiency (%) of (a) Z@Ag/TiO2, and (b) Z@Ag-	104
	La/TiO ₂ NPs towards different the concentrations of Cd ²⁺	
	against MB (constant), using 0.2 g of photocatalysts,	
	conducted at pH 6.8±0.2 and exposed under compact	
	fluorescent light for 3 h	
Figure 5.6	Proposed pathways for dyes degradation and metal ions	107
	reduction; (i) reduction of metal, (ii) and (iii) degradation of	
	dye, and (iv) dye excitation by visible light and de-excitation	
Figure 5.7	Equilibrium study of doped and undoped (a) TiO_2 ([MB] _o = 30	109
	mg/L), (b) zeolite supported TiO ₂ NPs ([MB] $_{o}$ = 150 mg/L),	
	using 0.2 g of photocatalysts, conducted at pH 6.8±0.1 and	
	exposed under compact fluorescent light for 3 h	
Figure 5.8	UV-Vis spectra of MB degradation onto doped and co-doped	112
	(a) TiO_2 ([MB] _o = 30 mg/L), and (b) zeolite supported TiO_2	
	NPs ([MB] _o = 100 mg/L), conducted at pH 6.8 \pm 0.1, exposed	
	under compact fluorescent light for 3 h	
Figure 5.9	Comparison of the removal efficiency of doped and undoped	115
	(a) TiO_2 ([MB] _o = 30 mg/L), and (b) zeolite supported TiO_2	

	NPs ([MB] _o = 150 mg/L), at pH 6.8 ± 0.1 and exposed under	
	compact fluorescent light vs in the dark for 3 h	
Figure 5.10	Pseudo-first order plots for the kinetic for the adsorption of MB	117
	using doped and undoped (a) TiO_2 ([MB] _o = 30 mg/L), (b)	
	zeolite supported TiO_2 NPs ([MB] _o = 150 mg/L), using 0.2 g	
	photocatalysts, conducted at pH 6.8±0.1 and exposed under	
	compact fluorescent light for 3 h	
Figure 5.11	Pseudo-second order plots for the kinetic for the adsorption of	119
	MB by using doped and undoped (a) TiO_2 ([MB] _o = 30 mg/L),	
	(b) zeolite supported TiO ₂ NPs ([MB] _o = 150 mg/L), using 0.2	
	g photocatalysts, conducted at pH 6.8±0.1 and exposed under	
	compact fluorescent light for 3 h	
Figure 5.12	Intraparticle diffusion model plots of (a) TiO ₂ and Ag/TiO ₂	123
	([MB] _o = 30 mg/L), and (b) zeolite supported Z@TiO ₂ and	
	$Z@Ag/TiO_2 ([MB]_o = 150 mg/L)$	
Figure 5.13	Intraparticle diffusion model plots of (a) Ag-La/TiO2 and	124
	La/TiO_2 ([MB] _o = 30 mg/L), and (b) zeolite supported Z@Ag-	
	La/TiO_2 and $Z@La/TiO_2$ ([MB] _o = 150 mg/L)	
Figure 5.14	Langmuir adsorption isotherm plots for the adsorption of MB	126
	onto (a) TiO_2 and Ag/TiO_2 , and (b) $Ag-La/TiO_2$ and La/TiO_2	
	NPs, using 0.2 g of photocatalysts, conducted at pH 6.8±0.1	
	and exposed under compact fluorescent light for 3 h	
Figure 5.15	Langmuir adsorption isotherm plots for the adsorption MB	127
	onto zeolite supported TiO ₂ NPs using 0.2 g of photocatalysts,	
	conducted at pH 6.8±0.1 and exposed under compact	
	fluorescent light for 3 h	
Figure 5.16	Freundlich isotherm plots of doped and undoped (a) TiO2, and	131
	(b) zeolite supported TiO ₂ NPs using 0.2 g of photocatalysts,	
	conducted at pH 6.8±0.1 and exposed under compact	
	fluorescent light for 3 h	

Figure 5.17	FT-IR spectra of doped and undoped (a) TiO2, and (b) zeolite	133
	supported TiO ₂ NPs after the degradation of MB, at pH 6.8±0.1	
	and exposed under compact fluorescent light for 3 h	
Figure 5.18	The comparative efficiencies of regenerated doped and	139
	undoped TiO ₂ NPs for the degradation MB (30 mg/L) via (a)	
	high temperature combustion, and (b) Fenton oxidation	
Figure 5.19	The comparative efficiencies of regenerated doped and	140
	undoped zeolite supported TiO2 NPs for the degradation MB	
	(150 mg/L) via (a) high temperature combustion, and (b)	
	Fenton oxidation	

LIST OF ABBEREVIATIONS

A Anatase

AAS Atomic Absorption Spectrophotometer

B Brookite

CB Conduction Band

DRS Diffused Reflectance Spectroscopy

E% Percent Efficiency

EDX Energy Dispersion X-ray

FT-IR Fourier Transform Infrared Spectroscopy

GPR General Purpose Reagent

HOMO Highest Occupied Molecular Orbital

LI Liquid Impregnation

Ln Lanthanide

LUMO Lowest Unoccupied Molecular Orbital

M Metal

MB Methylene Blue

NPs Nanoparticles

pH_{PZC} pH of Point of Zero Charge

R Rutile

RE Rare Earth

SEM Scanning Electron Microscopy

TEM Transmission Electron Microscopy

UV-Vis Ultraviolet and Visible

VB Valence Band

wt% Weight Percent

XRD X-ray Diffraction

XRF X-ray Fluorescence Spectrometer

Z Zeolite

PENYINGKIRAN FOTOKATALITIK METILENA BIRU TERSOKONG DARIPADA LARUTAN AKUEUS OLEH Ag DAN La TERDOP TiO2 DAN ZEOLIT

ABSTRAK

Dalam kajian ini, nanozarah (NPs) titanium dioksida (TiO2) diubahsuai melalui pendopan dengan Ag, La dan Ag-La menggunakan kaedah kos rendah dan impregnasi cecair mudah (LI), pemegunan keatas zeolit dan suhu pengkalsinan berbeza (500, 700 dan 900 °C). TiO2 NPs tanpa sokongan (TiO2, Ag/TiO2, Ag-La/TiO₂, dan La/TiO₂) yang disediakan pada suhu pengkalsinan yang berbeza, menunjukkan fasa anatas yang dominan (96-98 wt%), pengurangan tenaga luang jalur daripada 3.2 kepada 2.88 eV, dan pH_{PZC} antara 6.2 hingga 7.3. Sampel TiO₂ NPs tersokong zeolit (Z@TiO₂, Z@Ag/TiO₂, Z@Ag-La/TiO₂, dan Z@La/TiO₂) menunjukkan kemunculan fasa rutil dan brukit yang mencapai sehingga 20 wt% dengan peningkatan suhu pengkalsinan, pengurangan tenaga luang jalur dari 3.11 ke 2.90 eV dan nilai pH_{PZC} lebih tinggi (7.1-7.8) berbanding TiO₂ NPs tanpa sokongan. Penguraian fotokatalitik MB oleh TiO2 NPs tanpa sokongan dan tersokong zeolit dijalankan dalam keadaan makmal biasa iaitu pada pH sekitaran, suhu bilik (25±2 °C) dan lampu padat berpendarfluor. Oleh kerana zeolit meningkatkan keupayaaan penjerapan TiO2 NPs, kepekatan asal MB, [MB], berbeza digunakan bagi TiO2 NPs tersokong zeolit dan tanpa sokongan iaitu 200 dan 50 mg/L masing-masing. Didapati keupayaan penjerapan maksimum TiO2 NPs tersokong zeolit adalah antara 60 hingga 64 mg/g dan nilai tersebut lebih tinggi berbanding TiO2 NPs tanpa sokongan iaitu antara 13.6 hingga 19.4 mg/g. Model kinetik tertib kedua dan isoterma Langmuir adalah terbaik untuk menerangkan data fotodegradasi MB. Pencirian fotokatalis yang telah digunakan menggunakan teknik FT-IR, EDX dan XRF menunjukkan bahawa fotodegradasi MB berlaku melalui penjerapan pada permukaan fotokatalis. Kajian penggunaan semula TiO2 NPs tersokong zeolit dan tanpa sokongan menunjukkan bahawa kaedah guna semula fizik iaitu pembakaran pada suhu tinggi (530±20 °C) berkesan untuk memulihkan tapak aktif TiO2 NPs berbanding kaedah guna semula kimia iaitu pengoksidaan Fenton. Secara umum dan keseluruhannya, pendopan dengan Ag dan Ag-La meningkatkan aktiviti fotokatalitik TiO2 terubahsuai berbanding TiO2 tulen. Kesan ion saingan Cd²⁺, sebagai pemerangkap elektron terhadap penyingkiran MB adalah kurang nyata bagi TiO2 tersokong zeolit. Walau bagaimanapun, penambahan Cd²⁺ meningkatkan keupayaan penyingkiran TiO2 tanpa sokongan sebanyak 2.5 kali ganda.

PHOTOCATALYTIC REMOVAL OF METHYLENE BLUE FROM AQUEOUS SOLUTION BY Ag AND La DOPED TiO2 AND ZEOLITE SUPPORTED TiO2 UNDER VISIBLE LIGHT

ABSTRACT

In the present study titanium dioxide (TiO₂) nanoparticles (NPs) were modified via Ag, La and Ag-La doping using low cost and facile liquid impregnation (LI) method, immobilization on zeolite, and at different calcination temperatures (500, 700 and 900 $^{\circ}$ C). The unsupported TiO₂ NPs (TiO₂, Ag/TiO₂, Ag-La/TiO₂, and La/TiO₂) prepared at different calcination temperatures, showed dominant anatase phase (96 to 98 wt%), reduction of band gap energy from 3.2 to 2.88 eV, and pH_{PZC} between 6.2 to 7.3. The zeolite supported samples (Z@TiO2, Z@Ag/TiO2, Z@Ag-La/TiO2, and Z@La/TiO₂) prepared at different calcination temperatures, showed the appearance of rutile and brookite phases which reached up to 20 wt% with the increase in calcination temperature, less reduction in band gap energy (3.11 to 2.90 eV) and higher pH_{PZC} values (7.1 to 7.8) as compared to the unsupported TiO₂ NPs. The photocatalytic degradation of MB by unsupported and zeolite supported TiO2 NPs were performed under normal laboratory condition which is at ambient pH, room temperature (25±2 °C) and compact fluorescent light. Since the immobilization onto zeolite improved the adsorption capacities of the TiO₂ NPs, different initial concentrations of MB, [MB]₀, were used for unsupported and zeolite supported TiO2 which are 200 and 50 mg/L, respectively. It was observed that the maximum adsorption capacities of zeolite supported TiO2 NPs ranged between 60 to 64 mg/g and the values are comparatively higher than the unsupported TiO2 NPs which are between 13.6 to 19.4 mg/g. The pseudo-second order kinetic and Langmuir isotherm models are best to describe the MB photo-degradation data. The characterizations of the spent photocatalyst using FT-IR, EDX and XRF techniques, showed the photo-degradation of MB took place via adsorption of MB on the surface of the photocatalysts. The regeneration study of zeolite supported and unsupported TiO₂ NPs showed that the physical regeneration method using high temperature combustion method (530±20 °C) was effective to recover the active sites of TiO₂ NPs as compared to the chemical regeneration method, Fenton oxidation. In general and throughout, doping with Ag and Ag-La improved the photocatalytic activities of the modified TiO₂ compared to the pure TiO₂. The effect of competitive ions Cd²⁺, as electron trapper, towards MB removal was less obvious for the zeolite supported TiO₂. However, the addition of Cd²⁺ increased the removal capacities by almost 2.5 fold for the unsupported TiO₂ NPs.

CHAPTER 1

INTRODUCTION

1.1 Background

In recent years, the growing population and rapid industrial development have caused a steady increase in water pollution globally due to the higher discharge of harmful compounds. Water pollution has been ranked among the top rising social, political and economic challenges of today (Howell, 2013). As the need for clean water increases day by day, the demand for new remediation technologies which are environmentally friendly, grows. Researchers are aiming to efficiently fulfil the needs, and develop new processes for sustainable and eco-friendly water treatment technologies.

The textile industry is one of the largest pollutants contributor to surface and ground water resources, due to the large amount of water consumed during various textile manufacturing and processing. For example, the specific water consumption, to fabricate various textile products are approximately 932 L/kg depending on fiber type (Ozturk et al., 2016). Similarly, a large number of chemicals such as acids, bases, stabilizers, dispersing agents, complexing agents, surfactants, emulsifiers, enzymes, retarders, salts, solvents, fixing agents and dyes, are required to impart various desired properties to textile fibers (Le Marechal et al., 2012). An estimated dyestuff and supplementary consumptions in European Textile Industry alone are about 10 to 50 g/kg and 58 to 670 g/kg of the product, respectively (Ozturk et al., 2016). It is estimated that, during textile product processing more than 50 % of these chemicals are directly discharged in the textile effluent (Khatri et al., 2015).

Meanwhile, among the large number of pollutants in water, heavy metals such as Cd, Cu, and Ni with their non-biodegradable nature have a permanent influence and impact on the environment and human, and must be removed before being discharged into the water bodies (Mahdavi, 2016). Industrial development and human activities are the main sources of metal contamination (Jalbani & Soylak, 2014). Heavy metals enter human body through consumption of contaminated food, air, and water and hence damage living tissues of various organs such as kidney, liver and brain (Mahdavi, 2016). These metal ions are toxic even at very low concentrations such as 0.1–0.3 mg/L (Lai et al., 2010). Thus, choosing a suitable method for the removal of these heavy metal ions from contaminated water and improving its quality to a safe level is the main interest of many researchers. Various methods such as sorption (Ming et al., 2016), ion exchange (Cardoso et al., 2016), membrane filtration (Alothman et al., 2015), reverse osmosis (Petrinic et al., 2015), solvent extraction and electrolysis (Zamani et al., 2013), have been used to treat polluted water.

Previously, the traditional treatment methods (physical, chemical and biological treatment) have been widely used for the removal of organic pollutants such as dyes and heavy metals. However, each of these treatment methods has its own limitations. For example, the biological treatment is not very effective for the refractory synthetic dyes, which are resistant to aerobic bio-degradation (Mahmoodi & Arami, 2009; Spagni et al., 2010). The physical treatment methods such as adsorption, filtration or coagulation/flocculation are usually effective, but these treatment methods usually have high operational costs and suffers from post treatment of the solid and coagulated wastes (Akyol et al., 2004; Baldrian et al., 2006). Similarly, the chemical treatment has shortcomings such as the production of lethal and carcinogenic by-products, low efficiency, incomplete mineralisation and the

requirement of large amount of chemicals (Koprivanac & Kušić, 2009; Somensi et al., 2010). All the above mentioned methods have their own limitations, thus the development of a significantly better method for wastewater treatment is of utmost importance for long-term environmental viability.

Heterogeneous photocatalysis using titanium dioxide (TiO₂) is an effective technique for wastewater treatment, especially for the removal of non-biodegradable pollutants such as refractory organic dyes (Ertugay & Acar, 2016) and heavy metals (Mahdavi, 2016). Titanium dioxide NPs is widely used for the degradation and the mineralization of organic compounds to water and CO₂ without side-reactions (Chan et al., 2011). Similarly, it has a key role in the reduction of heavy metals to insoluble and significantly less toxic state, with subsequent recovery and removal of the metals from industrial effluents (Mahdavi, 2016). Titanium dioxide NPs has been proven to be the best photocatalyst among all other semiconductors due to its high efficiency, less toxicity, eco-friendliness, low cost, easily availability, highly oxidizing photogenerated holes and high stability in a wide range of pH and robustness to various wavelengths of radiation (Chan et al., 2011; Hashimoto et al., 2005; Somensi et al., 2010). However, some of the drawbacks of the titania are: the wide band gap (anatase phase = 3.2 eV) requires UV irradiation for activation, high photo-generated charge (electron-hole pair) recombination rate, anatase to rutile phase transformation and inefficient separation from aqueous medium, regeneration and reutilization (Han et al., 2009).

The presence of noble metals such as silver (Ashkarran et al., 2011), gold, palladium or platinum (Maicu et al., 2011), rare earth such as La, Gd or Eu (Li et al., 2008), and support materials such as zeolite (Kamegawa et al., 2013), SiO₂ (Hou et al., 2008) or chitosan (Kuwahara et al., 2009) have been reported to enhance the

photocatalytic activity of TiO₂. Noble metals act as electron trapper for photogenerated charge on the surface of TiO₂ and enhance the photocatalytic performance of TiO₂ (Dozzi et al., 2009; Yogi et al., 2009). For example, modification with silver ions (Ag⁺) reduces the electron-hole (e⁻-h⁺) recombination and this improves the photo-activity of TiO₂ (Behnajady et al., 2008). Rare earth metals enhance the photocatalytic efficiency of TiO₂ by reducing the rutile phase transformation, reducing the photo-generated charge recombination and shifting the absorption wavelength to visible region (Li et al., 2008). Similarly, the unique properties of support materials such as zeolite (Kamegawa et al., 2011) and chitosan (Kuwahara et al., 2009) have been intensively used in the design of TiO₂ photocatalyst for various applications. The surface modification of TiO₂ with a supporting material of hydrophobic nature such as zeolite can effectively enhance its efficiency and recovery from aqueous medium (Kamegawa et al., 2011; Kuwahara et al., 2009).

1.2 Problem Statements

Despite of the numerous advantageous characteristics of titania there are some limitations, which impede its photocatalytic efficiency. The bulk titania have a relatively wide band gap (3.0 eV for rutile and 3.2 eV for anatase), therefore, the photoexcitation of titania is restricted to only UV light irradiations, which is less than 10% of the total energy radiated from the sun. Secondly, the fast rate of photo-generated charge recombination limits the application of TiO₂ photocatalyst to a great extent. Also, the anatase phase of TiO₂ is more photo-catalytically efficient as compared to the rutile phase which is a more stable phase of TiO₂. The anatase to rutile phase transformation significantly decrease the photocatalytic efficiency of TiO₂ nanoparticle. Previous findings have shown that the introduction of various metals or non-metal impurities (doping) profoundly enhances the efficiency of TiO₂

photocatalyst by reducing the band gap, shifting the working wavelength to visible region, reducing the charge recombination and the phase transformation.

The aggregations of TiO₂ NPs in aqueous medium due to the high surface energy of particles also decreases the active surface, thus reducing the photocatalytic efficiency. Previously it was reported that the modification of TiO₂ with noble metals still suffers from aggregation effects which severely limit its efficiency and reutilization (Vi, 2005). The regeneration and reutilization of TiO₂ NPs from aqueous medium is difficult and the post-reaction filtrations or separations are both time and energy consuming processes. The choice of solid support and its inertness is always of paramount interest, because the TiO₂ photocatalyst not only mineralize the organic materials (pollutants) but also the organic support material matrices in which the NPs are supposed to be embedded. In addition, usually the main synthesis procedure of TiO₂, require large amount of alkoxide precursors and organic solvents. However, the yield of the end products is considerably low for the bulk treatments processes. Therefore, the need for a simple, cheaper and efficient procedure for the preparation of TiO₂ NPs is essential, to extend its applications to various fields where large amount of photocatalyst is required.

1.3 Objectives of the Proposed Work

- I. To prepare Ag, Ag-La and La doped TiO₂ NPs using a low cost and facile liquid impregnation method.
- II. To immobilize undoped and doped TiO₂ photocatalyst on zeolite and compare the effects of immobilization on the physico-chemical properties and efficiency of undoped and doped TiO₂ NPs.

- III. To identify various parameters to induce visible light activity to TiO₂ photocatalyst via doping with silver (Ag) and lanthanum (La) individually, and co-doping with Ag and La, immobilization on zeolite, calcination temperature as well as competitive ions, Cd²⁺, on the physico-chemical properties and the photocatalytic efficiency of TiO₂ towards Methylene Blue.
- IV. To study the kinetic and mechanism of photocatalytic degradation of MB.
- V. To study and evaluate the regeneration and reusability of doped and undoped TiO₂, and zeolite supported of TiO₂ photocatalysts.

CHAPTER 2

LITERATURE REVIEW

2.1 Photocatalysis

Photocatalysis is a catalytic process in which highly reactive species i.e. radicals or intermediates are formed in the presence of semiconductor that utilises light as the source of energy. These transitory species possess high oxidizing power and can speed up the degradation process of numerous organic and inorganic pollutants to complete mineralization in aqueous medium (Howell, 2013). The word "photocatalysis" was first used by Doerffler and Hauffe (1964) to describe the oxidation of CO using ZnO under light. However, when Fujishima and Honda reported water-splitting by using titanium dioxide, the work attained global academic recognition for TiO₂ as photocatalyst (Fujishima & Honda, 1972). Since then, heterogeneous photocatalysis has been employed in large number of applications in various fields.

Similar to conventional heterogeneous catalysis, the heterogeneous photocatalytic process follows the following steps (Pichat et al., 1989): (i) transfer of reactants to the surface of the catalyst; (ii) adsorption of the reactant onto the surface of the catalyst; (iii) reaction on the adsorbed phase; (iv) desorption of the product; and (v) removal of the product from the interfacial region. The photocatalytic reaction occurs in the adsorbed step, and the only difference between conventional catalysis and photocatalysis is that the thermal activation is replaced by photonic activation.

Photocatalyst is defined as a material that is capable of absorbing light irradiation and producing electron-hole pairs, that enable chemical transformations of the reactants and regenerate its chemical composition after each cycle of such

interactions (Khan et al., 2015). The significant features of the photocatalytic system are the desired band gap, suitable morphology, high surface area, stability and reusability (Hisatomi et al., 2014; Hoffmann et al., 1995). Researchers have shown that metal oxides such as TiO₂ and ZnO can be used as photocatalyst to decompose toxic organic compounds (Uddin et al., 2008), photovoltaic cells (Giordano et al., 2016), prevent fogging of glass (Khan et al., 2015) and even splitting of water into hydrogen and oxygen (Hisatomi et al., 2014). According to Rajeshwar (1995), for practical applications the semiconductor photocatalysts should have the following features: (i) photoactive, (ii) proficient to utilize visible and/or near-UV light, (iii) chemically and biologically inert, (iv) photo-stable and (v) inexpensive. In addition, the metal oxide semiconductors should be ecologically friendly and prepared via inexpensive routes (Choi, 2016; Khan et al., 2015).

Semiconductors are classified into two groups based on their photo-generated electronic transitions; (i) direct band gap semiconductors; and (ii) indirect band gap semiconductors (Ruzicka, 2013). In direct band gap semiconductors, the maximum energy states of valence band (VB) and the minimal energy state of conduction band (CB) has the same momentum, where the direct transition of electrons occurs frequently. However, in indirect band gap semiconductors, the VB maximal and the CB minimal bands do not have the same momentum and direct transitions of electrons are forbidden. Similarly, in direct band gap semiconductors charge recombination occur by direct recombination without change in momentum, while in indirect band gap semiconductors charge recombination occurs by changing the momentum (Ruzicka, 2013; Diesen, 2013), as described in Figure 2.1. The indirect recombination exhibits longer lifetime of charges (electron-hole pair) as compared to direct recombination (Ruzicka, 2013).

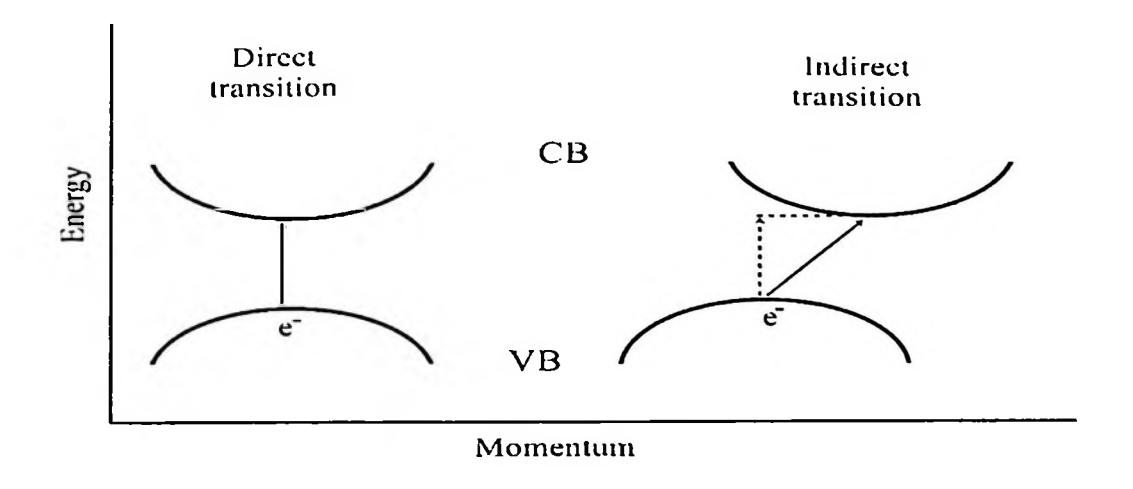


Figure 2.1. Schematic band structure of crystalline TiO₂ for direct and indirect electronic transitions

Generally, there are some chemical and technological requirements for safe and efficient cleansing methods. The photocatalytic system requires three fundamental elements which are the catalyst, light source and reactor configuration (Thiruvenkatachari et al., 2008). Among semiconductors such as ZnO (E_g=3.43 eV), ZnS (Eg=3.6 eV), WO₃ (Eg=2.76 eV), CdS (Eg=2.58 eV), and Fe₂O₃ (Eg=2.3 eV) etc, TiO₂ (anatase, E_g=3.2 eV) is extensively used for photocatalysis due to its high chemical stability, low cost and non-toxic nature (Augugliaro et al., 1988; Sakthivel et al., 2000; Thiruvenkatachari et al., 2008; Wu, 2004). ZnO shows effective photocatalytic decomposition towards organic pollutants, but unlike TiO2, ZnO is unstable during light irradiation which results in deactivation with time and ultimately decreases its photocatalytic efficiency (Carraway et al., 1994; Litter, 1999). CdS suffers from photo-corrosion mostly when the spectral response is to longer absorption wavelength, while Fe₂O₃ and WO₃ show good activity in visible range but their photocatalytic activity is less as compared to TiO₂ (Fox & Dulay, 1993; Reutergådh & Iangphasuk, 1997). Similarly, due to lower photo-stability and poor photocatalytic activity, ZnS has not received much attention like other semiconductors (Jinkai, 2007).

2.2 Titanium Dioxide

Titanium dioxide NPs have been proven to be the best photocatalyst among other semiconductors (Choi, 2016; Fujishima et al., 2000; Thiruvenkatachari et al., 2008). Generally, TiO₂ exists in three different crystallographic phases i.e. rutile, anatase and brookite. Some of the previous findings showed that the comparative phase stability is dependent on particle sizes (Zhang & Banfield, 2000). As the particle sizes decreases (i.e. < 11 nm), anatase is the most stable phase, while rutile is the most stable phase when particles are larger than 35 nm (Ranade et al., 2002; Zhang & Banfield, 2000, 2005). Meanwhile, the most suitable particles size is between 11-35 nm for brookite phase, although contradictory results have been presented and the variation of phases was found to be dependent on other factors as well (Fujishima et al., 2008; Zhang & Banfield, 2005).

All three phases are composed of the basic building unit TiO₆ octahedral configuration bound in different ways (Carp et al., 2004). The assembly patterns and the distortion of octahedral structures distinguish the crystallites of polymorphs from each other. Rutile phase is the most thermodynamically stable of the three phases, and formed by the edge-sharing of neighbour TiO₆ units to form long chains, while the anatase phase is composed of mainly point-sharing octahedra (Figure 2.2) and brookite phase is made up of a combination of edge and point-sharing (Carp et al., 2004; Diebold, 2003). Due to its instability, difficulty in synthesizing reliably and wide range of temperature, the brookite phase of titania is not often used for its structure analysis (Fuijshima et al., 2008; Primo et al., 2011).

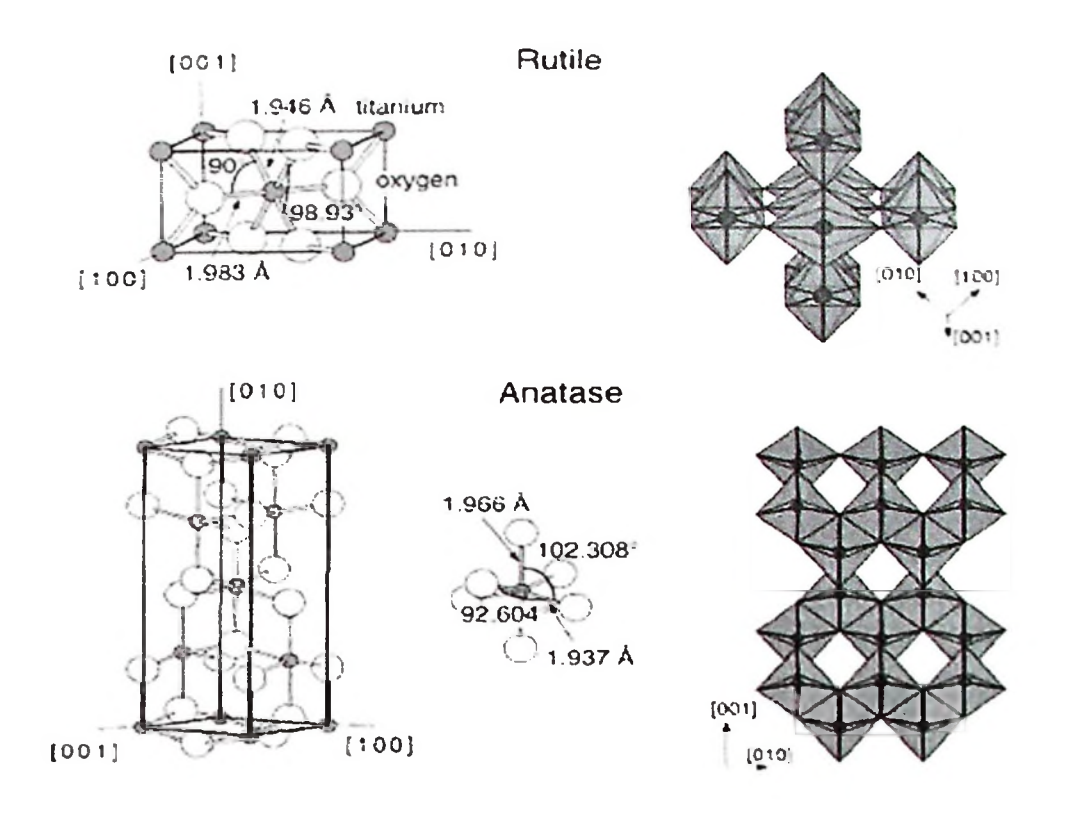


Figure 2.2. Bulk structures of rutile and anatase TiO₂ (Diebold, 2003).

Among the three crystalline phases of TiO₂, anatase is more efficient in photocatalytic applications due to its open structure as compared to rutile phase (Ibhadon & Fitzpatrick, 2013). The rutile phase also shows photocatalytic activity but to a lesser extent. However, brookite phase is uncommon, unstable and generally does not show appreciable photo-activity (Ibhadon & Fitzpatrick, 2013; Han et al., 2009). The higher photo-activity of anatase phase compared to rutile has been accredited to a higher hydroxylation of the surface which facilitates adsorption of oxygen in the form of O²⁻ or O⁻ (Vi, 2005).

Due to the small band gap energy (3.0 eV), the rutile phase of TiO₂ is a direct band gap semiconductor as compared to the anatase phase which is an indirect band gap semiconductor with the tendency for hole trapping on the particle surface (Colbeau-Justin et al., 2003; Hurum et al., 2003).

As a typical semiconductor, TiO₂ retains completely occupied VB and totally CB. The VB and CB are separated by a forbidden band gap energie (E_{bg}) (Hu et al., 2010). The absorption of a photon by TiO₂ with energy greater than or equivalent to its band gap energy can excite the electron from the completely filled VB into the empty CB, generating an excited electron (ē_{CB}) in the CB and positive charge hole (h̄_{VB}) in the VB. The photo-generated charge on titania further follow of one of the two possible mechanisms (Colbeau-Justin et al., 2003; Hurum et al., 2003; Meng-Hsiung et al., 2009): (i) reaction between the charge pair (electron-hole) and an electron accepter or donor, (ii) de-excitation/recombination of electron-hole pair, either as direct band gap semiconductor or indirect band gap semiconductor.

2.3 Modifications of TiO₂

Some limitations of TiO₂ can be overcome by modifying the surface of TiO₂. Tailoring of the surface can influence the optical and electrical properties of TiO₂ NPs which are crucial for industrial and commercial applications. Modifications of the TiO₂ mainly comprises of doping with metals and non-metals (Choi, 2016; Ramacharyulu et al., 2014; Han et al., 2009), dye sensitization (Chowdhury et al., 2012), and coupling with the lower band gap semiconductors (Daghrir et al., 2013), as discussed in the following sections.

2.3.1 Doping

The electronic structure of materials is mainly responsible for its optical response. The electronic properties describe the chemical composition of a particular nanomaterial. Doping is a procedure to introduce small amounts of impurities (foreign elements) to a semiconductor in order to modify its electronic properties by creating mid-gap states within the band gap of a material. As titania consist of titanium and

oxygen, it is more difficult to replace O²- anion with other anions due to its small ionic radii and difference in the charge. However, it is easier to replace Ti⁴⁺ cation with other transition element (Chen & Mao, 2007). The advantageous aspect to modify the nanomaterials is their small size which is responsible for high degree of tolerance in electronic structure distortion as compared to bulk materials (Bessekhouad et al., 2004; Burda et al., 2003).

The photocatalytic activity of doped titania is dependent on the dopant concentration, dopants d-electronic configuration, energy level of dopants in titania lattice, distribution of dopants in titania lattice, electrons donor concentration and the light intensity used for photocatalysis (López et al., 2001). The incorporation of metal cations as a guest to the nano-crystalline TiO₂ is responsible for many beneficial aspects such as reduction in band gap, reducing the electron-hole pair recombination, avoiding the collapse of the mesoporous framework, high porosity, active sites on the surface and reduction of rutile to anatase phase transformation (Venkatachalam et al., 2007).

The dosage amount of dopants is an important factor influencing the photocatalytic activity of TiO₂. For example, below the optimum level noble metal dopants can act as charge (electron-hole pair) separation centers and thus enhance the photocatalytic activity of modified TiO₂. Conversely, as the dosage amount exceeds the optimum level, the noble metals can act as charge recombination centers, where the reduction in photocatalytic activity occurs (Han et al., 2009).

Meanwhile, the effects of doping TiO₂ with non-metals and metals are different. Doping with non-metals tends to increase the VB maximum energy level, as most of the non-metallic dopants are less electronegative as compared to lattice oxygen. However, metallic element dopants tend to reduce the CB minimum energy

level, as most of the metal dopants are more electronegative than titanium (Nuramdhani, 2011). The photo-response of dopants modified semiconductors were such that the photons of energy (E) greater than band gap energy (E_{bg}), can possibly excite the electrons from VB to mid band gap states if it lies above the Fermi level or from the mid band gap states to the CB if it lies below the Fermi level (Ruzicka, 2013), as shown in Figure 2.3.

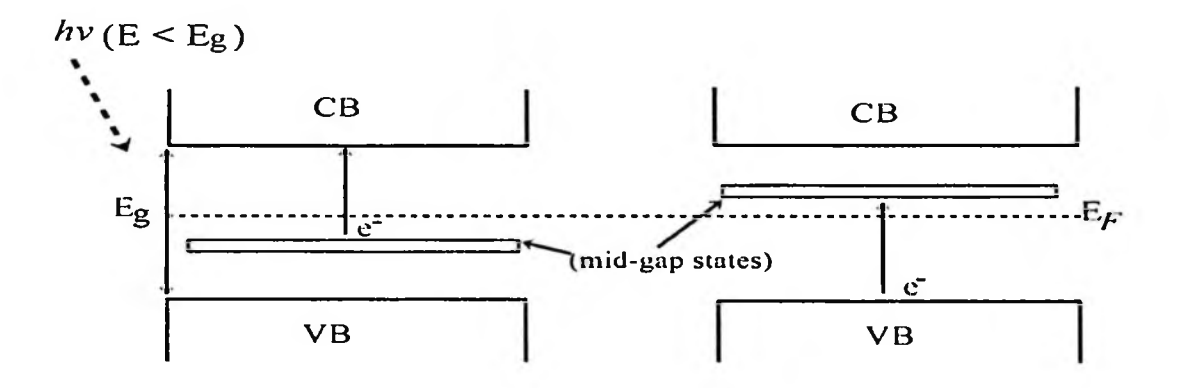


Figure 2.3. Schematic representation of mid band gap energy state and Fermi level (E_F) (Ruzicka, 2013)

Modifications of TiO₂ by doping are mainly divided into three groups, (i) anionic doping, (ii) cationic doping, and co-doping and these are described in detail in the following sections.

2.3.1(a) Anionic (Non-metals) Doping

The anions doping on TiO₂ lattice have attracted considerable interest due to the reduction in band gap and the shifting of absorption wavelength to visible light. The theoretical and experimental investigations by Asahi and co-workers, (2001) contributed to the understanding of the modifications of TiO₂ visible light driven photocatalyst. Their results showed that N dopant was most effective due to the mixing of 2p-orbital of N with 2p-orbitals states of O from TiO₂ which contributes by

narrowing the band gap as compared to other dopants (S, P or C). Although, S-doping shows narrowing of band gap, it is difficult to introduce sulfur atom into the TiO₂ lattices due to its larger size. Similarly, C and P exist deep in the band gap states of TiO₂, so it is difficult to transport photo-excited electrons to reactive sites within their lifetime (Asahi et al., 2001).

In addition, among anionic dopants, fluorine (F) produces numerous advantageous effects including: (i) the creation of surface oxygen vacancies, (ii) the enhancement of surface acidity, and (iii) the increase of Ti³⁺ ions (Li et al., 2005). Although, non-metals doping with TiO₂ reduces the band gap and shift the absorption wavelength significantly to visible region. However, low dopant levels of non-metals (<2 atomic %) can rigidly shift up the valence band (Fujishima et al., 2008; Serpone, 2006). For example, 20% N doping was required to mix the N 2p-orbital state with the O 2p-orbital valence band, but in preparation such a high dopants amount would resulted in the formation of TiN instead (Fujishima et al., 2008; Ozaki et al., 2005). The main problem present with non-metal doped TiO₂ photocatalyst is that the photocatalytic efficiency under visible light is lower as compared to under ultraviolet light (Fujishima et al., 2008).

2.3.1(b) Cationic (Metals) Doping

Cationic or metal doping occurs by replacing the Ti⁴⁺ centre in the TiO₂ crystal lattice, either by hybridising with the 3d-like conduction band of TiO₂ or by introducing new bands into the band gap (mid band gap state) (Tong et al., 2012). The densities of states (DOSs) calculations conducted by Umebayashi et al. (2002) showed that when titania was doped with metals such as V, Cr, Mn, Fe, or Co, an electron occupied energy level was formed and the electrons were localized around each dopant. As the atomic number of the dopant metal increases, the localized energy level

formed by the electrons are shifted to lower energy (Chen & Mao, 2007). Previously it was reported that a red shift in band gap transition was observed, which significantly activated the photocatalyst working range to visible light. For example, metal dopants such as Fe, V, or Mn, shifts the absorption spectra to the lower energy region and the absorption in visible region increases with an increase in the dopants concentration (Choi et al., 1994; Luo & Gao, 1992; Wang et al., 1999). This red shift was due to the charge transfer between the dopants d electrons and the CB or VB of TiO₂ (Chen & Mao, 2007).

Meanwhile, the modifications of TiO₂ NPs by using noble metals such as Ag, Au, Pt and Pd, as guest phase cations highly favoured the enhancement of photocatalytic activity (Fujishima et al., 2008; Hirakawa & Kamat, 2005; Maicu et al., 2011). The alteration of TiO₂ stem with noble metals can facilitate the photocatalytic activity of TiO₂ by the following reasons (Bessekhouad et al., 2004; Hirakawa & Kamat, 2005; Jakob et al., 2003):

- (a) reduction in band gap and shifting the absorption wavelength to visible region by photo-exciting surface plasmons;
- (b) charge transfer between VB and CB;
- (c) act as electron trap and thus increase electron-hole pair charge separation;
- (d) enhanced the interfacial electrons transfer rate.

For example, silver doping to TiO₂ has been found effective in enhancing the quantum efficiency of the photocatalyst due to the transfer of photo-generated electron to Ag particles because of the lower Fermi level of Ag. Similarly, the crystalline defects within TiO₂ lattice formed by doping Ag favours photo-generated electrons capture. The fine crystallized TiO₂ anatase phase can facilitate the transfer of the

photo-generated electron from bulk to surface, thus lowering the probability of photoinduced holes and electrons recombination (Han et al., 2009).

Modifications with lanthanide metals or rare earth (Ln(III) such as La, Ce, Er, Pr. Gd. Nd. and Sm) have also been reported to significantly modify the electrical, physical and chemical properties of TiO₂ photocatalyst (Li et al., 2008; Li et al., 2004; Zhang et al., 2004). Lanthanide metal ions play an effective role in tailoring the TiO₂ surface for various photocatalytic applications. The formation of lanthanides metal ions complexes with various Lewis bases such as amines, aldehydes, alcohols, thiols, etc, involves the f-orbital electrons which provide effective substrate for the adsorbability of organic pollutants and improve the photocatalytic activity of TiO₂ (Li et al., 2008). The characteristics 4f, 5d electronic configuration of lanthanides metal ions alter the optical and catalytic properties of TiO₂ by producing labile oxygen vacancies of fairly high charges mobility and by redox coupling of Lnⁿ⁺/Ln⁽ⁿ⁻¹⁾⁺ than the bulk oxygen species of TiO2 lattice (Zhang et al., 2004). Since the ionic radii of rare earth metals are larger than Ti⁴⁺ ion they are deposited on the surface of TiO₂, which increases the effective surface area of TiO₂ photocatalyst (Li et al., 2004). Doping with lanthanide metal ions has been reported to reduce the agglomeration of TiO₂ particles in aqueous medium and enhance the photocatalytic efficiency (Ruifen et al., 2015). Hence, this increases the availability of active surface areas and enhanced the photocatalytic activity. The incorporation of lanthanide metal ions in TiO2 lattice acts as electrons trapper and reduces electron-hole recombination rate of semiconductor photocatalyst (Li et al., 2008). According to Li et al. (2004) the Ln-(III) doping to TiO2 were effective to inhibit the anatase to rutile phase transformation, enhance the thermal stability, reduce the crystallite size, and increase the surface Ti³⁺ content.

2.3.1(c) Co-doping

Doping with metals and non-metals has been found to produce advantageous effect to TiO₂ by reducing absorption threshold and harvesting solar light as source of activation. However, sometimes dopant act by itself as a recombination centre thereby reducing the charge separation and increasing the rate of electron-hole pairs recombination in mono-doped TiO₂ (Cong et al., 2007; Sakatani et al., 2004). Monodoping may disturb the periodic lattice structure of TiO₂ photocatalyst (Chen et al., 2010). Besides acting as visible light absorption source, these impurity states act as charge carrier traps for the photo-induced e-/h+ pairs. Therefore, the rapid transportation of photo-generated charge in TiO₂ requires visible light active states in the energy gap to sufficiently overlap with the band states (VB and CB) of TiO2 photocatalyst (Chen et al., 2010; Han et al., 2009). However, it has been shown earlier by Asahi et al. (2001) that these mono-dopants active states are located deeply in the band gap of TiO2, to efficiently couple with the intrinsic bands of semiconductor photocatalyst (Asahi et al., 2001). To reduce the limitations of mono-doping and improve the photocatalytic activities of TiO₂ NPs, co-doping has been found beneficial in shifting these impurity states and enhancing the electronic interface between the TiO₂ intrinsic bands and impurity states and the other possible way is to introduce different dopants to TiO₂ nano-matrix (Chen et al., 2010).

The modification of TiO₂ NPs with binary components (co-dopants) to prepare a three junctions i.e. co-doped photocatalyst, has already been tested. The photocatalytic activities of these three junctions photocatalyst were observed to be higher when compared to the pure TiO₂ or one component doped TiO₂ system (Han et al., 2009). The cooperative actions of the co-dopants were observed when the Fe³⁺ dopant served as photo-generated hole trap while Eu³⁺ acted as photo-generated

electrons scavenger in TiO2. According to the authors, the presence of both ions accelerated the anodic and cathodic processes by increasing the interfacial charge transfer (Yang et al., 2002). Wei and co-workers (2004) observed part of O vacancies of Ti₅O₉ in La-N co-doped TiO₂ NPs were occupied by N due to the same p-orbital electronic configuration of oxygen (of TiO2 lattice) and nitrogen, which is responsible for the decrease in the band gap of doped TiO₂. The co-doped La³⁺ ions prevented the aggregation of powder in the process of nitrification and increased the surface area of the nano-catalyst (Wei et al., 2004). Meanwhile, the incorporation of metals such as Ag, Ce, Fe, La-cations and N anion co-dopants in TiO₂ lattice significantly shift the absorption wavelength to visible region and enhanced the photocatalytic activity. The researchers claimed that metal cations with radius larger than the radius of Ti⁴⁺ such as Ag were incorporated in the bulk phase and were uniformly distributed in the interstices of TiO₂ lattice. Meanwhile, due to smaller ionic radii the Fe³⁺ cations are present inside the titania lattice due to partial replacement with the Ti⁴⁺ lattice (Zhongqing et al., 2007). In particular, the band gaps decreased to a large extent by dopant cations having smaller radii than that of Ti⁴⁺ (Shi et al., 2007).

Self-doping or the production of Ti³⁺ species inside TiO₂ nano-materials has been found as an alternate means of extending the photo-response of titania (Amano et al., 2013; Zhang et al., 2013; Zuo et al., 2010). The Ti³⁺ species are generally formed by oxygen vacancies in the material, which results in the creation of a localised midgap state, approximately 0.75–1.18 eV below the conduction band edge (Zuo et al., 2010). However, these oxygen vacancies also act as bulk defects which increase the rate of recombination, and any benefit from doping must be considered against this (Ruzicka, 2013).

2.3.2 Modifications with Dye Sensitization and Coupling

Recently the photo-sensitization of TiO2 semiconductor by organic dye with visible light absorbing chromophores has been reported (Chowdhury et al., 2012). Dye sensitization mechanisms involves the photo-excited dye injecting charge into the conduction band of semiconductor producing oxidized dye radical. The dye acted as sensitizer as well as substrate to be degraded (Han et al., 2009). The photo-activity of dye sensitized mechanism is based on the absorption of visible light by dye, resulting in an excitation of highest occupied molecular orbital (HOMO) electron to the lowest unoccupied molecular orbital (LUMO), and transfer of electrons to the CB of TiO₂ while the dye itself is transformed into cationic radical. In this process TiO₂ acts as mediator for the transfer of electrons from dye (sensitizer) to the substrate present on TiO₂ surface as electron accepter, while the electrons in the valence band remain unchanged. The injected electrons from the dye jump over quickly to TiO2 surface where the molecular oxygen scavenged these electrons and form superoxide radicals O₂ and hydrogen peroxide radicals OOH (Chowdhury et al., 2012; Pan et al., 2011; Pelaez et al., 2012). These reactive radical species can also disproportionate to form hydroxyl radicals OH. The photocatalytic route of dye sensitization enhanced the efficiency from the fact that it can consume an ideal energy source (solar light), which is free and unlimited. However, the limitation with dye sensitized TiO2 is the effect of different dopants on the self-photosensitized dyes degradation in dye/TiO2 under visible light irradiation is limited as compared to under UV irradiation (Han et al., 2009).

The wide band gap of TiO₂ restricts photo-induced electron-hole pairs to reach the interface between semiconductor photocatalyst and water, where the photocatalytic degradation takes place. To overcome this problem TiO₂ were coupled with small band

gap semiconductors such as ZnO, CdS, CuO, SnO₂, CdSe etc, to reduce the electronhole pairs recombination rate and enhance the photocatalytic activity (Fujishima et al., 2008; Khan et al., 2015). Metal oxide and TiO2 composites have high potential to shift the working wavelength to visible light, resulting in the enhancement of photocatalytic activities by inducing the synergetic effects which inhibit the electron-hole recombination rate and compensate the limitations of individual component (single dopant) effects (Pelaez et al., 2012). The effective electron-hole pairs charge transfers between the coupled semiconductors (sensitizer) and TiO₂ mainly depend upon the difference between the VB and CB potentials of the two semiconductors (Han et al., 2009; Pelaez et al., 2012). The TiO₂ valence and conduction bands potentials should be less positive and more negative than the coupled sensitizer. Meanwhile, the conduction band potential of a sensitizer (narrow band gap semiconductor) should be higher and its valence band should lower than the valence band of TiO₂ semiconductor. The larger the differences between the band potentials of two semiconductors the greater will be the interfacial charge transfer (Fujishima et al., 2008; Han et al., 2009; Pelaez et al., 2012).

2.3.3 Modifications via Calcination Temperature

The effect of calcination temperature on the physico-chemical properties of TiO₂ and photocatalytic activity depend upon various aspects such as methods of preparation, dopants (modifications with metals or non-metals) and treatments of substrate/pollutants i.e. photocatalytic reaction conditions. Previously, Moon et al. (2001) reported that the photocatalytic activity was maximum for sample calcined at 500 °C due to the complete crystallization of the anatase phase at this temperature. The catalytic activities of non-metal dopants such as N- and F-TiO₂, decreased noticeably with the increase in the calcination temperature from 500 to 700 °C (Akpan & Hameed,

2009; Huang et al., 2007). When Du et al. (2008) compared the effects of calcination temperature of Degussa P25 and rare earth (RE) metals doped TiO₂, and they observed that the photocatalytic efficiency of P25 Degussa calcined at 600 °C was higher than that of RE doped TiO₂ under UV irradiation. However, the trend reversed for the sample calcined at 800 °C under the same condition (Du et al., 2008). The trend on the influence of calcination temperature on the removal of MB under UV irradiation by using N-doped TiO₂ are in the following order: 300 > 500 < 700 °C (Huang et al., 2007). Although anatase and rutile phase exist in tetragonal structure, experimental evidence indicates that anatase is more stable kinetically than rutile at room temperature and atmospheric pressure (Pillai et al., 2007). Meanwhile, rutile phase was reported to be more stable thermodynamically than anatase at normal temperature (Periyat et al., 2008). Theoretical calculation by Zhang and Banfield (2005) showed that the anatase phase of titania was transformed to rutile only after the crystallite size grew to ~14 nm, while below this critical size the anatase phase was more stable.

Earlier, Bickley and co-workers (1991), proposed that the rutile phase with smaller band gap energy (3.0 eV) acted as "electron-sink" and increased the charge recombination rate and therefore was not suitable for photocatalytic applications. The findings by Colbeau-Justin et al. (2003) revealed that the rutile phase acted as passive electron trap for photo-generated electron on anatase in biphasic anatase-rutile mixture, which reduces the life time of the charges. Therefore, in mix rutile-anatase phase the rapid recombination may not favour the enhancement in photo-activity (Colbeau-Justin et al., 2003). However, Hurum et al. (2003) suggested that in mixed-phase materials, the electron transfer occurs from rutile to the lower energy trapping sites of anatase phase and this prolong the life-time of photo-generated charge. The findings showed that the mixed phase photocatalyst effectively enhance photocatalytic

activity (Hurum et al., 2003). Figure. 2.4 explains the statements of Bickley's and Hurum's theory.

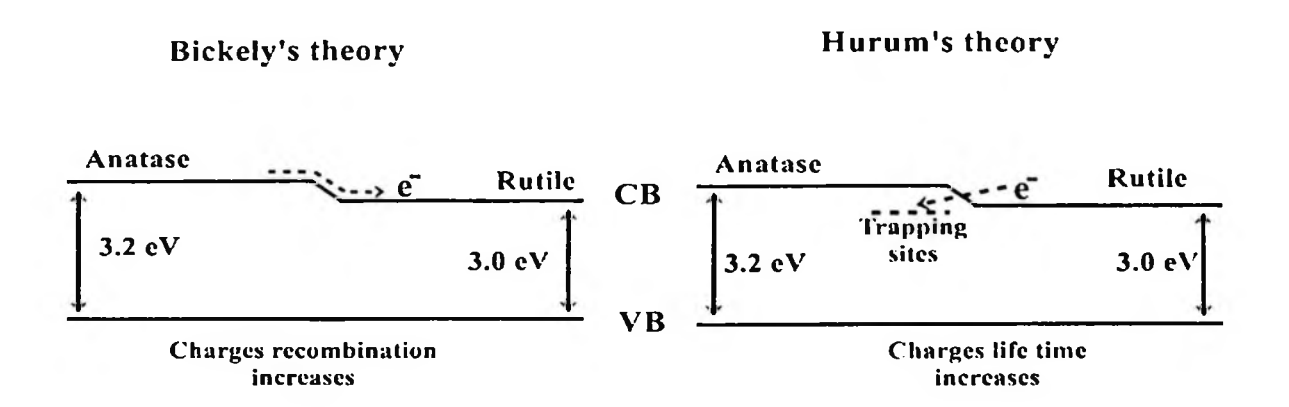


Figure 2.4. Schematic representation of Bickley's (Bickley et al., 1991), and Hurum's theories (Hurum et al., 2003)

The Degussa P25 generally contains biphasic mixture of rutile-anatase and has shown greater photocatalytic activity than pure anatase phase (Shen et al., 2011). Several attempts to study the synergistic effects of mixed phases, such as anatase-rutile, rutile-brookite and anatase-brookite, revealed the evidence of enhanced photocatalytic efficiency (Shen et al., 2011; Su et al., 2011). This enhancement in photocatalytic efficiency is attributed to the increase in charge separation by biphasic mixture as compared to the mono-phasic TiO₂.

2.4 Immobilization of TiO₂ onto Solid Support

The nano-sized powdered photocatalysts possess a large surface area to volume ratio which make them highly desirable for catalytic reactions. Large number of pollutants with a higher concentration can be adsorbed and decomposed on the surface of the nano-sized photocatalyst. Since heterogeneous photocatalysis mainly occurs in aqueous medium, the dispersion and stabilization of the nano-sized photocatalyts in aqueous medium is a big problem in different processes. The sedimentation of the

nano-sized particles increases considerably with the increase in the dispersion of the powder in aqueous medium (Yaremko et al., 2001). Similarly, the major drawback with nano-powder catalysts are the separation of the spent catalysts from liquid phase. The nano-powder samples require costly separation techniques, in addition to the post reaction separation ability which increases the time and energy consumption, and also reduces the regeneration and reutilization of catalyst. In order to avoid the costly separation step, extensive efforts have been dedicated to the fixation of nanoparticle photocatalysts on different solid substrates such as SiO₂ (Kamegawa et al., 2011), activated carbon (Zhang et al., 2010), alumina (Habibi et al., 2012), zeolite (Zhao et al., 2015) and chitosan (Kuwahara et al., 2009).

The choice of solid support material is of great importance as the introduction of foreign material i.e. support material may also cause some undesirable effect on the photocatalytic activity of the catalyst (Fernandez et al., 1995). The photocatalytic activity of the material is directly dependent on the immobilization technique and the consequent sintering processes which significantly effects the physical and chemical properties of the photocatalyst. The important characteristics while choosing a good support for TiO₂ are the stability of the material i.e. chemical inertness, surface area and hydrophilic or hydrophobic properties (Alwash et al., 2013; Diesen, 2013).

Various support materials have been widely used to modify and enhance the photocatalytic activity of TiO₂. However, the support materials sometime reduce the photocatalytic efficiency due to following reasons (Carp et al., 2004; Fernandez et al., 1995; Ibhadon & Fitzpatrick, 2013):

- Reduction of the active surface of photocatalyst;
- Mass transfer limitations;